

Highly flexible whole-field sectioning microscope with liquid-crystal light modulator

S Monneret, M Rauzi and P-F Lenne

Institut Fresnel, UMR 6133 CNRS-Université Paul Cézanne Aix-Marseille III, Domaine Universitaire de Saint-Jérôme, 13397 Marseille Cedex 20, France

E-mail: serge.monneret@fresnel.fr

Received 1 November 2005, accepted for publication 17 January 2006

Published 7 June 2006

Online at stacks.iop.org/JOptA/8/S461

Abstract

We present a cheap and flexible whole-field sectioning microscope based on a structured illumination technique for fluorescence biological imaging. A programmable liquid-crystal-based dynamic mask produces a patterned illumination in order to generate sectioned images of a thick sample. Sectioning strengths ranging between 0.45 and 7.5 μm are obtained depending on the spatial frequency of the displayed grid pattern. As an example of biological application, images of *Drosophila*'s embryo, optically sectioned in different z -planes 1 μm apart, are shown. We also discuss the basic theory of structured illumination microscopy considering in detail the frequency mixing process required to shift signals into the microscope's optical transfer function domain.

Keywords: structured illumination, fluorescence microscopy, Fourier optics

(Some figures in this article are in colour only in the electronic version)

1. Introduction

Fluorescence microscopy has become a basic technique in the field of modern biology thanks to the development of new labelling methods and of new fluorescent dyes. This optical system, like any others, presents limited spatial resolution. In recent years patterned-excitation-based techniques, such as laterally modulated excitation microscopy (LMEM [1]), structured illumination microscopy [2] and harmonic excitation light microscopy (HELM [3]), have been introduced to increase the spatial resolution of conventional wide-field microscopy. All these methods are based on a frequency mixing process capable of enlarging the domain of the optical transfer function (OTF) of the microscope. Thanks to this process, additional components of the object spectrum are shifted inside the microscope's OTF domain: the resulting effect is an improved spatial resolution produced by the spectral transfer of a region of sample information away from the spectrum obtained by using conventional flat illumination [4, 5].

Pattern excitation technique can be also used to produce optical sectioning with an improved axial resolution

comparable to the one obtained with a confocal microscope. The new system, pioneered by Neil *et al* in 1997 [6] and capable of high axial resolution, is obtained by modifying the conventional illumination of a fluorescence microscope in order to project a single spatial frequency grid pattern directly onto the object: the grid pattern will then be efficiently imaged only on those portions of the specimen that are in focus. We can therefore obtain an optically sectioned image of a specimen by extracting fluorescence light information coming from the modulated slice. The grid pattern can be finally removed by acquiring and numerically processing a set of three spatially modulated wide-field images, where, for each one of them, the grid is laterally translated by a third of its period. Structured illumination sectioning microscopy has been tested in white-light microscopy [6], fluorescence microscopy [7] and fluorescence lifetime microscopy [8–10] and experimentally used in reflectance-mode imaging on a thick biological specimen [11]. A structured illumination optical sectioning microscope was recently produced and commercialized by Zeiss and by Thales Optem under the names of ApoTome [12] and of OptiGrid [13], respectively.

In the mentioned optical sectioning systems a solid grid produces light modulation providing a single fixed optical sectioning strength. In order to make the system reconfigurable and tunable it is possible to use dynamic masks that permit highly flexible pattern frequency variation providing a dynamic sectioning capability. Up to now, only one tunable sectioning system, based on a computer-controlled digital micromirror device, has been presented [14].

This paper presents an alternative tunable structured light sectioning system that produces light modulation thanks to a liquid-crystal-based dynamic mask that generates illumination patterns under programmable control: sectioning strategies, depending on experimental conditions, can thus be easily planned. The paper is structured in two sections: section 2 reviews the theory given by Neil *et al* [6] in order to compare differences between the two structured illumination techniques, the one improving lateral resolution and the one producing optical sectioning. Particular emphasis is given to the frequency mixing process required to shift signals into the microscope's OTF domain. Section 3 presents the experimental set-up, the software implementations that make possible full control of the system built and the resulting sectioning strength achieved. The last topic of this section presents the sectioning capability of our system. The structured illumination sectioning microscope was tested on biological samples: sectioned images of a fixed and fluorescently labelled *Drosophila* embryo are shown.

2. Optical sectioning in fluorescence microscopy by using structured excitation light

2.1. Principle

2.1.1. Fluorescence imaging of thick specimens. In fluorescence light microscopy, incoherent image formation is obtained by convolving the specimen's distribution of emitted light intensity with the point spread function h of the microscope, i.e. the image of a point source of light.

Considering the case of an infinitely thin sample placed on the plane $z = z_0$ and assuming a $1 \times$ optical magnification, the recorded intensity distribution of fluorescence light $\theta(x, y)$ on the CCD camera is given by

$$\theta(x, y) = \int_{\text{focus on } z_0} \int_{-\infty}^{\infty} \Phi(x', y', z_0) \times h(x - x', y - y', z_0) dx' dy', \quad (1)$$

which can also be written $\theta(x, y)_{\text{focus on } z_0} = \Phi(x, y, z_0) \otimes h(x, y, z_0)$, where $\Phi(r)$ is the distribution of the fluorescence light intensity.

It is possible to extend equation (1) to the case in which a thick specimen is taken into consideration [15]:

$$\theta(x, y) = \int_{\text{focus on } z_0} \int_{\Delta z} \Phi(x, y, z) \otimes h(x, y, z - z_0) dz \quad (2)$$

where Δz is the support of the fluorescence function Φ on the z axis, and where $h(x, y, z - z_0)$ denotes that the point spread function strongly depends on the distance from the focus plane.

The basic relation, describing the fluorescence emission rate of isotropically distributed fluorophores for any polarization state of the exciting light, can be easily expressed by

$$\Phi(x, y, z) = A\psi(x, y, z) \cdot I(x, y, z), \quad (3)$$

where ψ is the density of fluorophores in the specimen, I the excitation light distribution and A a constant related to the quantum efficiency of the fluorophores. This expression shows how the distribution of fluorescence light is modulated by the excitation intensity I before being imaged by the microscope. For a thick fluorescent specimen we can therefore deduce, considering equations (2) and (3), that a non-negligible amount of light, coming from planes out of focus, produces a blur effect on the recorded image.

By modulating the specimen with a structured excitation light, a frequency shift of fluorescent light information signals is obtained. This process allows recovery of additional components of the object spectrum by displacing them into the microscope's OTF domain. The spectral translation can lead to an improved lateral resolution, after adapted post-processing [4], or to optical sectioning if the shift brings the spectral information in a wanted spectral position in order to benefit from the optical sectioning property of the microscope's OTF.

2.1.2. Structured excitation as a way to shift spectral images in Fourier space. Structured excitation light microscopy is a technique based on a spatially modulated intensity pattern projection onto a specimen, generating a harmonic frequency mixing process.

The resulting intensity modulation $I(x, y, z)$ of the excitation light on the focus plane is given by

$$I(x, y, z = z_0) = I_0 \cdot (2 + C_x \cos(2\pi\sigma_0 x - \Phi_x) + C_y \cos(2\pi\mu_0 y - \Phi_y)), \quad (4)$$

where I_0 is the uniform intensity distribution, σ_0 and μ_0 are the spatial frequencies defining the pattern, C_x and C_y are contrast coefficients, Φ_x and Φ_y are phase constants that displace the pattern in x and y directions, respectively.

Spatial extension of $I(x, y, z)$ on the z -axis is directly correlated to the depth of focus of the objective lens. An equivalent description of $I(x, y, z_0)$ on the focus plane can be given by

$$I(x, y, z_0) = \frac{I_0}{2} [4 + C_x e^{-j\Phi_x} e^{j2\pi\sigma_0 x} + C_x e^{j\Phi_x} e^{-j2\pi\sigma_0 x} + C_y e^{-j\Phi_y} e^{j2\pi\mu_0 y} + C_y e^{j\Phi_y} e^{-j2\pi\mu_0 y}] \quad (5)$$

which leads to the resulting image $\theta_{\Phi_x \Phi_y}(x, y)_{\text{focus on } z_0}$ on the CCD camera that can be expressed by

$$\theta_{\Phi_x \Phi_y}(x, y) = 2\theta_0(x, y) + \theta_{X-}(x, y)_{\text{focus on } z_0} e^{-j\Phi_x} + \theta_{X+}(x, y)_{\text{focus on } z_0} e^{j\Phi_x} + \theta_{Y+}(x, y)_{\text{focus on } z_0} e^{j\Phi_y} + \theta_{Y-}(x, y)_{\text{focus on } z_0} e^{-j\Phi_y} \quad (6)$$

where $\theta_0(x, y)$ is the image obtained with a uniform illumination and where $\theta_{X-}(x, y)$, $\theta_{X+}(x, y)$, $\theta_{Y-}(x, y)$ and $\theta_{Y+}(x, y)$ correspond to images whose spectrum is shifted by σ_0 and μ_0 along the σ and μ axes in positive and negative directions with respect to the original spectrum $\tilde{\psi}(\sigma, \mu)$. This can be easily seen considering each component in the bi-dimensional spatial frequency domain through the Fourier transform:

$$\tilde{\theta}_0(\sigma, \mu) = I_0 \int_{\text{focus on } z_0} \int_{\Delta z} \tilde{\psi}(\sigma, \mu, z) \cdot H(\sigma, \mu, z - z_0) dz \quad (7)$$

$$\tilde{\theta}_{X-}(\sigma, \mu) = \frac{I_0}{2} C_X \int_{\Delta z} \tilde{\psi}(\sigma - \sigma_0, \mu, z) \cdot H(\sigma, \mu, z - z_0) dz \quad (8)$$

$$\tilde{\theta}_{X+}(\sigma, \mu) = \frac{I_0}{2} C_X \int_{\Delta z} \tilde{\psi}(\sigma + \sigma_0, \mu, z) \cdot H(\sigma, \mu, z - z_0) dz \quad (9)$$

$$\tilde{\theta}_{Y-}(\sigma, \mu) = \frac{I_0}{2} C_Y \int_{\Delta z} \tilde{\psi}(\sigma, \mu - \mu_0, z) \cdot H(\sigma, \mu, z - z_0) dz \quad (10)$$

$$\tilde{\theta}_{Y+}(\sigma, \mu) = \frac{I_0}{2} C_Y \int_{\Delta z} \tilde{\psi}(\sigma, \mu + \mu_0, z) \cdot H(\sigma, \mu, z - z_0) dz \quad (11)$$

where H is the optical transfer function of the microscope and where the symbol \sim denotes a two-dimensional Fourier transform.

Thanks to spectral shifts, given by equations (8)–(11), additional high frequency regions of the optical spectrum are brought into the microscope's OTF domain. The four shifted spectra constitute the basis of one of the main applications of structured light: reconstruction of high resolution images in fluorescence microscopy [4]. In order to produce high resolution images in 2D, a grid pattern presenting modulation in both x and y direction is necessary: five wide-field images, with different phase offsets (ϕ_x and ϕ_y) corresponding to different positions of nodes and antinodes of the excitation pattern, must be acquired. These images must be numerically post-processed to extract each single component $\tilde{\theta}_0$, $\tilde{\theta}_{X+}$, $\tilde{\theta}_{X-}$, $\tilde{\theta}_{Y+}$ and $\tilde{\theta}_{Y-}$, finally rearranged to obtain the final high resolution image. In [5], phase offsets (on x and y axes respectively) are chosen to be $(0, 0)$, $(\pi/2, 0)$, $(\pi, 0)$, $(0, \pi/2)$ and $(0, \pi)$. The five spectra $\tilde{\theta}_0$, $\tilde{\theta}_{X+}$, $\tilde{\theta}_{X-}$, $\tilde{\theta}_{Y+}$ and $\tilde{\theta}_{Y-}$ are extracted by solving a 5×5 set of linear equations obtained from the Fourier transforms of the acquired images. Having defined the attenuation of the microscope's OTF, the five spectral components are shifted to a desired position and superimposed [5]. The final high resolution image is obtained by an inverse Fourier transform of the extended spectrum.

2.2. Optical sectioning

2.2.1. The optical transfer function of the microscope. Considering equations (7)–(11), we can affirm that the OTF of the microscope strongly influences the optical properties of the four spectral components $\tilde{\theta}_{X+}$, $\tilde{\theta}_{X-}$, $\tilde{\theta}_{Y+}$ and $\tilde{\theta}_{Y-}$ of the recorded image. Stokseth expression of the OTF [16] leads to the expression

$$H(\rho, \varepsilon) = K(\rho) J_{\text{inc}} \left[\frac{8\pi\omega(\varepsilon)}{\lambda} \left(1 - \frac{\rho}{f_c} \right) \frac{\rho}{f_c} \right] \quad (12)$$

where $K(\rho) = 1 - 1.38(\frac{\rho}{f_c}) + 0.034(\frac{\rho}{f_c})^2 + 0.344(\frac{\rho}{f_c})^3$; $\varepsilon = z - z_0$; $\rho = \sqrt{\sigma^2 + \mu^2}$; $J_{\text{inc}}(x) = 2\frac{J_1(x)}{x}$ with J_1 the first order Bessel function; $\omega(\varepsilon) \approx 2\varepsilon \sin^2 \frac{\alpha}{2}$ with $n \sin(\alpha)$ the numerical aperture (from [17]).

The second factor of function H , strictly related to the first order Bessel function, is directly responsible for optical sectioning. Figure 1 presents the function $H(\rho, \varepsilon)$ behaviour for a NA 1.4 oil-immersion objective lens: the graph shows that, in a conventional wide-field microscope, the zero spatial frequency is the only component of an image that is not attenuated with defocus. Neglecting factor $K(\rho)$, we can

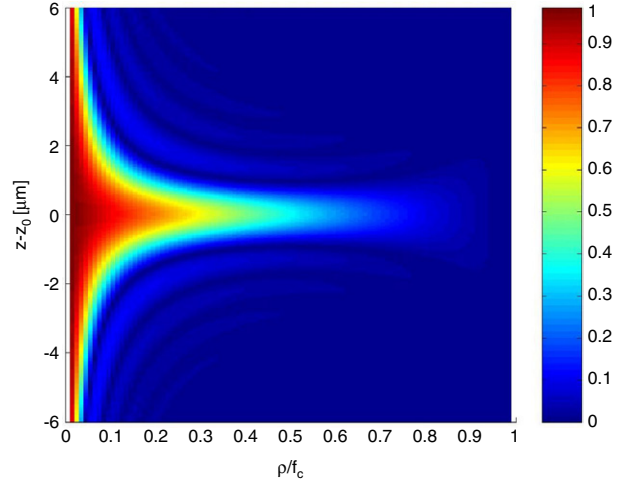


Figure 1. Example of $H(\rho/f_c, z - z_0)$ for an oil-immersion objective lens of NA = 1.4.

finally state that the maximal sectioning strength is achieved when a grid pattern, presenting a spatial frequency equal to $f_c/2$, is used. Considering now the entire H function with factor $K(\rho)$ behaving as a low-pass filter, we can say that the best compromise between good sectioning strength and correct transmission of the objective is achieved by using pattern modulations presenting a spatial frequency around $f_c/5$.

We can finally conclude that optical sectioning in wide-field fluorescence microscopy requires the spectral shift of images into the frequency domain defined by $\rho \in [\frac{f_c}{10}, \frac{f_c}{2}]$.

2.2.2. An easy method of obtaining sectioned images and removing the grid pattern. The expression of H , given by equation (12), indicates that optical sectioning only depends on the angle formed by light with respect to the optical axis. The simplest way to obtain optical sectioning consists in projecting simple grids on the sample, thus considering $\mu_0 = 0$. We then have

$$I(x, y, z = z_0) = I_0 \cdot (1 + C_x \cos(2\pi\sigma_0 x - \Phi_x)), \quad (13)$$

which leads to

$$\theta_{\Phi_x}(x, y) = \theta_0(x, y) + \theta_{X-}(x, y) e^{-j\Phi_x} + \theta_{X+}(x, y) e^{j\Phi_x} \quad (14)$$

The resulting optical transfer function of the structured illumination microscope is made up by three spectral components: the conventional OTF, centred in the Fourier domain, and two sideband copies of the OTF axially shifted by the spatial modulation. Equations (8) and (9) show that θ_{X+} and θ_{X-} are complex images of virtual fluorescent sources presenting the same fluorescence intensity distribution of the actual object. If spectral shifts along the σ axis are well adapted, we can finally obtain an optically sectioned image and remove the grid pattern by separating θ_{X+} or θ_{X-} from θ_{Φ_x} .

A set of linear equations must be solved in order to extract θ_0 , θ_{X+} and θ_{X-} : a set of three different images, named IM₁, IM₂ and IM₃, corresponding to three different spatial phase ϕ_x shifts, are used to solve such an equation system. Since

the specimen's fluorophore distribution on the focused plane is unknown, we must use shift vectors that make possible equal illumination of each portion of the sample. Noise is minimized in the final composite image if the shift vectors equally span the period of the lowest nonzero frequency component of the excitation field [18]: this can be achieved by setting for example the values of ϕ_x as $(\phi_1, \phi_2, \phi_3) = (0, 2\pi/3, 4\pi/3)$. We then obtain

$$IM_1(x, y) = |\theta_{\phi_1}(x, y)| \text{ with } \theta_{\phi_1}(x, y) = \theta_0(x, y) + \theta_{X-}(x, y) + \theta_{X+}(x, y) \quad (15)$$

$$IM_2(x, y) = |\theta_{\phi_2}(x, y)| \text{ with } \theta_{\phi_2}(x, y) = \theta_0(x, y) + e^{-j\frac{2\pi}{3}}\theta_{X-}(x, y) + e^{j\frac{2\pi}{3}}\theta_{X+}(x, y) \quad (16)$$

$$IM_3(x, y) = |\theta_{\phi_3}(x, y)| \text{ with } \theta_{\phi_3}(x, y) = \theta_0(x, y) + e^{-j\frac{4\pi}{3}}\theta_{X-}(x, y) + e^{j\frac{4\pi}{3}}\theta_{X+}(x, y). \quad (17)$$

By solving this set of equations we obtain

$$\theta_0(x, y) = \frac{1}{3}(\theta_{\phi_1}(x, y) + \theta_{\phi_2}(x, y) + \theta_{\phi_3}(x, y)) : \text{conventional wide-field image} \quad (18)$$

$$\theta_{X+}(x, y) = \frac{1}{3}(\theta_{\phi_1}(x, y) + e^{-j\frac{2\pi}{3}}\theta_{\phi_2}(x, y) + e^{j\frac{2\pi}{3}}\theta_{\phi_3}(x, y)) \quad (19)$$

$$\theta_{X-}(x, y) = \frac{1}{3}(\theta_{\phi_1}(x, y) + e^{j\frac{2\pi}{3}}\theta_{\phi_2}(x, y) + e^{-j\frac{2\pi}{3}}\theta_{\phi_3}(x, y)). \quad (20)$$

Considering $\tilde{\theta}_{X+}$ and $\tilde{\theta}_{X-}$ symmetry in Fourier space, the expression of the object's sectioned image IM_{sec} can be given by

$$IM_{\text{sec}}(x, y) = \frac{1}{3}|\theta_{\phi_1}(x, y) + e^{j\frac{2\pi}{3}}\theta_{\phi_2}(x, y) + e^{j\frac{4\pi}{3}}\theta_{\phi_3}(x, y)|, \quad (21)$$

which is analogous to the homodyne detection in communications systems. Alternatively, IM_{sec} can be given by [6]

$$IM_{\text{sec}}(x, y) = \{(IM_1(x, y) - IM_2(x, y))^2 + (IM_1(x, y) - IM_3(x, y))^2 + (IM_2(x, y) - IM_3(x, y))^2\}^{1/2}, \quad (22)$$

which is analogous to square-law detection.

Equation (22) gives the easy and practical way to compute IM_{sec} from the three recorded images IM_1 , IM_2 and IM_3 . Moreover the conventional wide-field image I_{WF} can be given by

$$I_{\text{WF}}(x, y) = \frac{IM_1(x, y) + IM_2(x, y) + IM_3(x, y)}{3}. \quad (23)$$

We can finally state that the conventional and the optically sectioned image can be obtained simultaneously from the same data.

3. Optical sectioning by using a liquid-crystal-based dynamic grid

3.1. Experimental apparatus

Our structured excitation light fluorescence microscopy process consists in illuminating the fluorescent sample with a one-dimensional grid-like pattern that is generated by a liquid-crystal-based spatial light modulator. The conventional fluorescence excitation light path of the microscope was

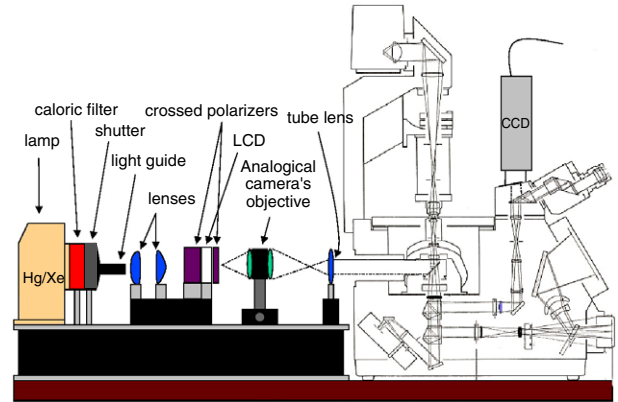


Figure 2. Schematic view of the additional structured illumination system used to obtain a flexible optically sectioning microscope from a conventional one.

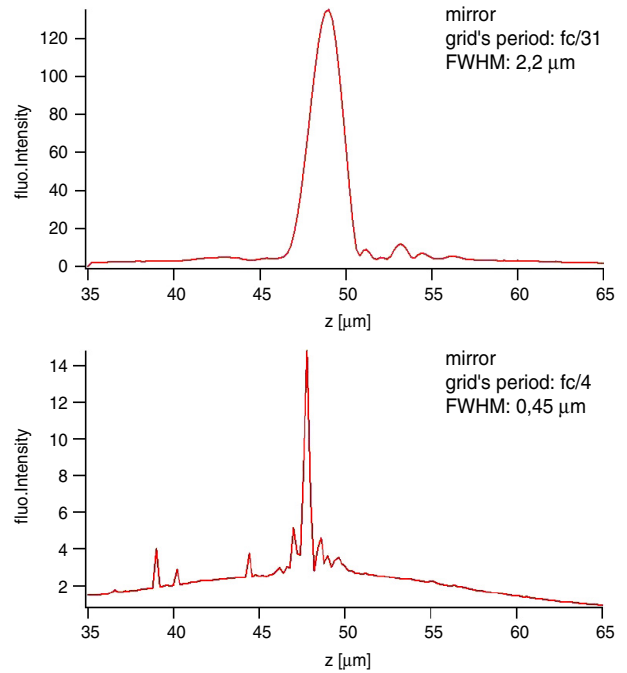


Figure 3. Variation of the fringe intensity level versus the position of the objective lens. The position of the mirror is set to $48 \mu\text{m}$.

modified in order to project any kind of pixel image by focalizing a dynamic mask onto the specimen (figure 2).

In the experimental apparatus we used a Zeiss Axiovert 35M inverted optical microscope supplied with a 63X infinitely corrected oil-immersion objective (Zeiss Neofluar, 1.4 NA), presenting a cut-off frequency f_c of 88 lines mm^{-1} . The objective was axially displaced by a PIFOC piezoelectric system capable of 10 nm resolution (Physik Instrumente, Germany). A Hg/Xe lamp (Hamamatsu, Japan) was used to provide the excitation light needed. A light guide was also used in order to make the system more flexible. The images of fluorescent specimens were recorded with a CCD camera (Kappa DX 2HC-FW, Germany) capable of a recording rate of 9 images s^{-1} .

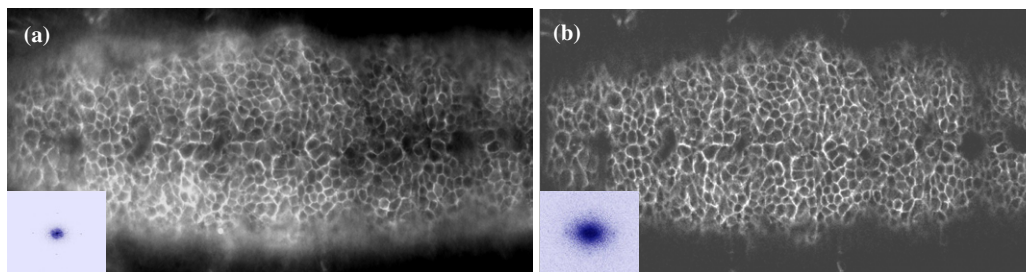


Figure 4. *Drosophila* embryo membrane labelled with Alexa488-Neurotactin: (a) without sectioning; (b) with a $6.4 \text{ lines mm}^{-1}$ spatial frequency grid sectioning pattern. The insets give the spatial spectra of the images.

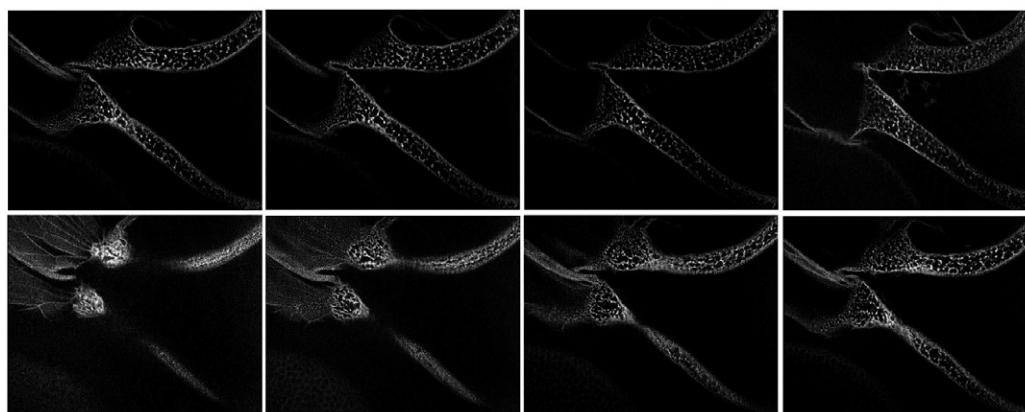


Figure 5. *Drosophila* embryo at a late stage of development. Sectioned images with $1 \mu\text{m}$ step between two successive records. Sectioning strength of $1 \mu\text{m}$, corresponding to a $6.4 \text{ lines mm}^{-1}$ spatial frequency grid pattern.

Table 1. Sectioning strengths and fluorescence peak intensity at the focus plane measured for various grid spatial frequencies.

Grid frequency on the LCD (lines mm^{-1})	No grid	fc/125	fc/62	fc/31	fc/15	fc/8	fc/4	fc/2
Experimental FWHM (μm)	23	7.5	4.1	2.3	1.1	0.9	0.45	—
Experimental peak intensity (arbitrary unit)	170	140	135	130	60	40	15	—

The dynamic binary mask used consists of a liquid crystal display (LCD) spatial light modulator (SLM) sandwiched between two crossed polarizing optics in order to enable the liquid crystals to act as an intensity modulator. The model used is a 33 mm diagonal poly-silicon TFT twisted nematic LCD, with a pixel pitch of $26 \times 26 \mu\text{m}^2$ (XGA2, CRL Opto Ltd., UK). The contrast ratio of the digital device is given as better than 100:1. The interface allows the SLM to be driven directly by the video adapter of a personal computer set to XGA resolution (1024×768 pixels) and running at a frame of 60 Hz.

Software for complete management of the sectioning process has been implemented. It controls and synchronizes all I/O devices (LCD imaging capability, PIFOC displacement, CCD camera's photo timing and shutter's mechanical aperture) and manipulates images, taken by the CCD camera, giving the sectioned image as output. The developed system is fully automated. Once all necessary images have been taken and stored in memory, the software is designed to exploit the calculus capacities of the personal computer to obtain the sectioned images (22).

3.2. Experimental results

3.2.1. Sectioning strength. An extremely thin specimen is necessary to define the sectioning strength of the system. After trying to use thin films of fluorescent material we found it easier and more practical to use a reflecting mirror. The emission light filter was removed to allow back-scattered excitation light to pass from the mirror to the CCD sensor. By sectioning the mirror (after choosing a grid frequency) on different z -planes a few hundreds of nanometres apart, it was easy to evaluate the sectioning strength. A curve giving the recorded brightness variation for the successive sectioned pictures versus z positions was plotted. The full width at half maximum (FWHM) of the picked resulting curve was finally said to represent the sectioning strength of the system (figure 3). The fact that minor peaks have been detected (see figure 3 at the bottom) is due to possible electronic noise of the CCD camera and to the imperfect light intensity stability coming from the excitation lamp. The sloping background represented in the same graphs is due to the zero order that, even if strongly reduced, has not been completely removed

from the images. Table 1 gives all experimental data obtained, that are the sectioning strength of the system, depending on the spatial frequency used, and the maximal fluorescence intensity of the curve (expressed in arbitrary units) showing the effect of the strong low-pass spatial filtering effect of the microscope's OTF.

3.2.2. Example of biological application. The structured light sectioning microscope was tested on *Drosophila* embryo membranes labelled with Alexa488-neurotactin (Molecular Probes, USA). Figure 4 shows the picture and the corresponding spectrum of the sample recorded without structured illumination (a), and sectioned with a $6.4 \text{ lines mm}^{-1}$ spatial frequency grid pattern (b). The spectra obtained are in agreement with the theoretical predictions: the spectrum of the sectioned image presents a considerable increase of the high frequencies of the specimen spectrum, which brings a better imaging of high frequency details. However, there is no absolute spectral extent of the sectioned image spectrum and thus no improvement of lateral resolution.

The goal of performing good sectioning is followed by the one of being able to achieve a high repetition rate of generated sectioned images. Timings of the system were analysed and optimized: the system was capable of whole-field sectioning strength ranging between 7.5 and $0.45 \mu\text{m}$ with a repetition rate of generated sectioned images, mainly limited by the frame rate of our CCD camera (9 frames s^{-1}), of 3 Hz . Figure 5 shows a *Drosophila* embryo, taken in its late stage of development, sectioned in different z -planes $1 \mu\text{m}$ apart with a CCD recording rate of 9 Hz .

4. Conclusion

A fully functional, automated and reconfigurable structured illumination sectioning microscope was assembled, characterized and tested on fluorescently labelled *Drosophila* embryos. We have presented the possibility of using a cheap LCD dynamic mask in order to produce optical sectioning using structured illumination. By projecting a grid onto the object and acquiring a set of three spatially modulated wide-field images with the grid translated by a third of its period, it is possible to compute a depth-resolved wide-field image at the focal plane in a sample. The sectioned images produced are similar to what would be obtained by using a confocal scanning microscope. Thanks to the dynamic mask, sectioning strength can be easily varied between $7.5 \mu\text{m}$ and 450 nm . The experimental set-up is simple to implement and works with almost any optical source. The LCD, simply interfaced by a video adapter, can be easily incorporated in a complete programmable process in order to automatically record complete stacks of sectioned images of thick biological specimens e.g. *Drosophila* embryos.

Acknowledgment

We thank Thomas Lecuit (IBDM, Marseille) for providing us with *Drosophila* embryos.

References

- [1] Heintzmann R and Cremer C 1999 Lateral modulated excitation microscopy: improvement of resolution by using a diffraction grating *Proc. SPIE* **3568** 185
- [2] Gustafsson M 2000 Surpassing the lateral resolution limit by a factor of two using structured illumination microscopy *J. Microsc.* **198** 82
- [3] Frohn J, Knapp H and Stemmer A 2000 True optical resolution beyond the Rayleigh limit achieved by standing wave illumination *Proc. Natl Acad. Sci.* **97** 7232
- [4] Gustafsson M 1999 Extended resolution fluorescence microscopy *Curr. Opin. Struct. Biol.* **9** 627
- [5] Fedoshev R, Belyaev Y, Frohn Y and Stemmer A 2004 Structured light illumination for extended resolution in fluorescence microscopy *Opt. Lasers Eng.* **43** 403
- [6] Neil M, Juskaitis R and Wilson T 1997 Method of obtaining optical sectioning by using structured light in a conventional microscope *Opt. Lett.* **22** 1905
- [7] Neil M, Squire A, Juskaitis R, Bastiaens P and Wilson T 2000 Wide-field optically sectioning fluorescence microscopy with laser illumination *J. Microsc.* **197** 1
- [8] Cole M, Siegel J, Webb S, Jones R, French P, Lever M, Sucharov L, Neil M, Juskaitis R and Wilson T 2000 Whole-field optically sectioned fluorescence lifetime imaging *Opt. Lett.* **25** 1361
- [9] Cole M *et al* 2001 Time-domain whole-field fluorescence lifetime imaging with optical sectioning *J. Microsc.* **203** 246–57
- [10] Webb S *et al* 2002 A wide-field time-domain fluorescence lifetime imaging microscope with optical sectioning *Rev. Sci. Instrum.* **73** 1898
- [11] Tkaczyk T, Rahman M, Mack V, Sokolov K, Rogers J, Richards-Kortum R and Descour M 2004 High resolution, molecular-specific, reflectance imaging in optically dense tissue phantoms with structured-illumination *Opt. Express* **12** 3745
- [12] ApoTome structured-illumination head, by Zeiss Inc. at www.zeiss.com
- [13] OptiGrid structured-illumination system by Thales Optem at www.thales-optem.com
- [14] Fukano T and Miyawaki A 2003 Whole-field fluorescence microscope with digital micromirror device: imaging of biological samples *Appl. Opt.* **42** 4119
- [15] Dey N, Boucher A and Thonnat M 2002 Image formation model of a 3-D translucent object observed in light microscopy *IEEE Image Process.* **2** 469
- [16] Stokseth P 1969 Properties of a defocused optical system *J. Opt. Soc. Am.* **59** 1314
- [17] Young I, Zagers R, van Vliet L, Mullikin J, Boddeke F and Netten H 1993 Depth-of-focus in microscopy *Proc. 8th Scandinavian Conf. on Image Analysis (Tromsø, Norway)* pp 493–8 (Norwegian Society for Image Processing and Pattern Recognition)
- [18] So P, Kwon H-S and Dong C 2002 Resolution enhancement in standing-wave total internal reflection microscopy: a point-spread-function engineering approach *J. Opt. Soc. Am. A* **18** 2833